Received: 2 December 2025 | Revised: 12 January 2026 | Accepted: 11 February 2026 | Published online: 28 February 2026

RESEARCH ARTICLE

Smart Wearable Technology
2026, Vol. 00(00) 1–9
DOI: 10.47852/bonviewSWT62028665

BON VIEW PUBLISHING

# Structural, Optical, and Nonlinear Optical Properties of ZnO Nanostructures Grown on Porous Silicon

**Marwa. K. Abood[1,*], Wafaa Khalid Khalef[1], Amenah Ali Salman[2], Nibras Salah Hameed[3] and Mohammed Khalid Khalaf[4]**

[1] *Applied Science College, University of Technology, Iraq*

[2] *Department of Communication Engineering, University of Technology, Iraq*

[3] *Ministry of Higher Education and Scientific Research, Iraq*

[4] *Department of Computer Engineering, Erciyes University, Turkey*

**Abstract:** Zinc oxide (ZnO) nanostructures were effectively produced on a porous silicon (PS) substrate using thermal evaporation, thereafter undergoing oxidation at 600 °C. The structural, morphological, elemental, optical, and nonlinear optical (NLO) characteristics of the synthesized films were methodically examined. X-ray diffraction research indicated that the ZnO/PS films possess a polycrystalline hexagonal wurtzite structure with a preferential orientation along the (101) plane, and the average crystallite size was calculated to be around 3.8 nm, affirming their nanocrystalline characteristics. Scanning electron microscopy pictures revealed the presence of agglomerated nanostructures and nanorods over the PS surface, signifying elevated surface roughness and extensive surface area. Energy-dispersive X-ray investigation verified the predominance of Zn and O, with modest contributions from Si originating from the substrate. The optical absorption spectra exhibited a significant blue shift attributable to quantum confinement phenomena, with the optical band gap measured at approximately 3.6 eV. The calculated Urbach energy ($E_u$ = 145 meV) indicates a moderate level of structural disorder and the presence of tail states near the band edge, aligning with the nanocrystalline characteristics of ZnO films. The Z-scan approach utilized for NLO measurements demonstrated saturable absorption behavior, suggesting possible applications in photonic and optical limiting devices.

**Keywords:** ZnO nanostructures, porous silicon, Urbach tail, nonlinear optics

## 1. Introduction

Nanostructured materials have emerged as a fundamental aspect of contemporary materials science owing to their distinctive physical, chemical, and optical properties that markedly differ from those of their bulk counterparts [1]. Their decreased dimensionality and substantial surface-to-volume ratio confer unique attributes that are greatly sought after for applications in photonics, optoelectronics, and sensing technologies [2]. Zinc oxide (ZnO) has emerged as a flexible and multifunctional semiconductor due to its wide direct band gap of 3.37 eV, substantial exciton binding energy of 60 meV, and exceptional transparency in the visible spectrum [3]. Moreover, ZnO demonstrates exceptional chemical stability, radiation resistance, and mechanical strength, rendering it a viable material for high-performance nanodevices [4]. The physical and optical properties of ZnO are significantly affected by its structural features, shape, and synthesis circumstances. Diverse deposition processes have been utilized to create ZnO nanostructures, including chemical vapor deposition [5], sol–gel processing [6], magnetron sputtering [7], pulsed laser deposition [8], and thermal evaporation [9]. Each approach offers unique benefits in regulating film crystallinity, grain dimensions, and surface morphology. The thermal evaporation technique provides a straightforward, economical, and vacuum-compatible approach for generating homogeneous ZnO nanostructures characterized by excellent purity and adjustable thickness [10].

Porous silicon (PS) has gained significant attention as a substrate material due to its extensive specific surface area, adjustable porosity, and unique optical properties, including low reflectivity and visible photoluminescence [11]. The characteristics of PS render it an excellent medium for the nucleation and growth of ZnO nanostructures. The deposition of ZnO onto PS can notably modify the interfacial properties, crystallinity, and defect density of the resulting composite, resulting in enhanced structural and optical responses [12]. These hybrid systems offer important insights into how oxide semiconductors interact with PS surfaces,

*Corresponding author: Marwa. K. Abood, Applied Science College, University of Technology, Iraq. Email: marwa.k.abood@uotechnology.edu.iq

which are essential for customizing the functional properties of nanocomposite films [13].

Recent studies have underscored the significance of nonlinear optical (NLO) properties in wide-band-gap semiconductors such as ZnO, which demonstrate phenomena including saturable absorption (SA) and nonlinear refraction. The observed effects stem from quantum confinement and energy levels associated with defects, thereby augmenting the material's applicability in photonic and optical limiting devices. Thus, comprehending the relationship between microstructure, morphology, and NLO response is crucial for enhancing ZnO-based nanostructures for cutting-edge photonic applications [14].

Recently, the rapid expansion of wearable technology has created an urgent need for semiconducting nanomaterials that combine high optical sensitivity, mechanical robustness, and compatibility with flexible substrates. ZnO is especially attractive for wearable devices due to its biocompatibility, piezoelectric response, ultraviolet (UV) sensitivity, and stability under repeated mechanical deformation. When integrated with PS, ZnO nanostructures benefit from enhanced surface area, efficient light–matter interaction, and improved charge transport pathways, all of which are highly desirable for wearable strain sensors, UV photodetectors, biomedical monitoring patches, and flexible optoelectronic components. Therefore, examining the structural, optical, and NLO characteristics of ZnO/PS nanostructures provides important insights into their potential implementation in next-generation wearable systems [15].

This investigation involved the synthesis of ZnO nanostructures on PS substrates through the thermal evaporation method, subsequently followed by thermal oxidation. The investigation focused on the structural, morphological, elemental, and optical characteristics of the prepared films using techniques such as X-ray diffraction (XRD), scanning electron microscopy (SEM), energy-dispersive X-ray (EDX) spectroscopy, and UV–Vis spectroscopy. Additionally, the NLO properties were assessed through the Z-scan technique to investigate their applicability in photonic applications. The results enhance our comprehension of the ways in which synthesis parameters and substrate morphology affect the physical and optical characteristics of ZnO/PS nanostructures [16].

## 2. Literature Review

Recent studies have underscored the significance of (NLO properties in wide-band-gap semiconductors such as ZnO, which demonstrate phenomena including SA and nonlinear refraction [14]. The observed effects stem from quantum confinement and energy levels associated with defects, thereby augmenting the material's applicability in photonic and optical limiting devices. Thus, comprehending the relationship between microstructure, morphology, and NLO response is crucial for enhancing ZnO-based nanostructures for cutting-edge photonic applications [15].

## 3. Research Methodology

### 3.1. Preparation of porous silicon substrate

PS layers were fabricated on p-type single-crystalline silicon wafers oriented in the (100) direction, exhibiting a resistivity of around 1–10 Ω·cm. Before the anodization process, the silicon substrates underwent ultrasonic cleaning in isopropyl alcohol, followed by rinsing in deionized water and air drying. The porous structure was created through electrochemical etching in an electrolyte solution consisting of 20% hydrofluoric acid combined with ethanol in a 1:2 volume ratio. The silicon wafer functioned as the anode, whereas a gold electrode served as the cathode. A current density of 15 mA/cm² was utilized for a duration of 20 min at ambient temperature. Throughout the etching process, the temperature of the electrolyte was kept below 25 °C to prevent bubble formation and to guarantee a consistent distribution of pores. Following the etching procedure, the samples underwent rinsing with ethanol and were subsequently dried using a nitrogen gas flow.

### 3.2. Deposition and oxidation of ZnO nanostructures

ZnO nanostructures were deposited on the prepared PS substrates utilizing the thermal evaporation technique at a vacuum pressure of around $1 \times 10^{-5}$ Torr. High-purity metallic zinc (99.9%) served as the evaporation source. The separation between the source and the substrate was maintained at approximately 15 cm to guarantee uniform film deposition. After deposition, the samples underwent oxidation in air at 600 °C for 4 h using a conventional quartz-tube furnace to achieve nanocrystalline ZnO. The oxidation process enabled the full conversion of the metallic zinc layer into ZnO nanostructures, exhibiting enhanced crystallinity.

### 3.3. Characterization techniques

The synthesized ZnO/PS nanostructures were analyzed for their structural, morphological, and compositional characteristics using various analytical tools.

1) X-ray diffraction (XRD): Measurements were conducted utilizing a Shimadzu XRD-6000 diffractometer with *Cu Kα* radiation ($\lambda$ = 1.5406 Å) across a $2\theta$ range of 20°–80°. The estimation of the average crystallite size was conducted utilizing the Scherrer equation.
2) Scanning electron microscopy (SEM): The surface morphology and distribution of nanostructures were examined utilizing a Tescan Vega II SEM system, which is integrated with an EDX spectrometer for the analysis of elemental composition.
3) Optical characterization: UV–Vis absorption spectra were obtained to assess the optical absorption edge and determine the optical band gap energy through Tauc's relation [17]. NLO measurements were conducted utilizing the Z-scan technique in both open- and closed-aperture configurations to analyze SA and nonlinear refraction behaviors.

## 4. Results and Discussion

The XRD pattern of the ZnO nanostructures deposited on the PS substrate is presented in Figure 1. The diffraction peaks corresponding to ZnO were XRD examination.

Figure 1 illustrates the XRD pattern of the ZnO nanostructures that have been deposited on the PS substrate. The diffraction peaks associated with ZnO were identified at $2\theta$ values of 34.6°, 36.4°, 47.6°, 56.8°, 63.3°, 68.2°, and 69.4°, which correspond to the (002), (101), (102), (110), (103), (112), and (201) planes, respectively. The observed peaks align well with the standard hexagonal wurtzite phase of ZnO (JCPDS card no. 36-1451), thereby confirming the effective oxidation of metallic Zn into crystalline ZnO. The observed diffraction peaks are in good agreement with the standard hexagonal wurtzite ZnO phase as reported in the JCPDS

**Figure 1**
**XRD pattern of ZnO film deposition on PS**

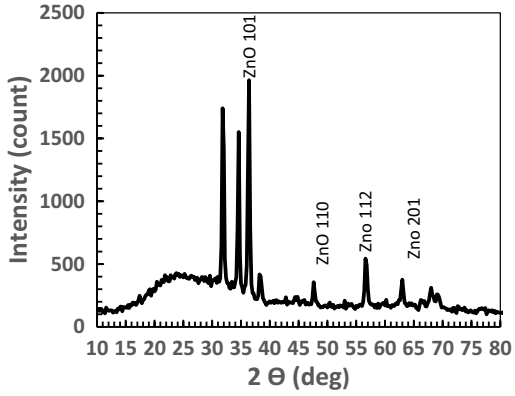


database (card no. 36-1451), confirming the phase purity of the synthesized ZnO nanostructures. A subtle diffraction peak at 38.6° was linked to residual metallic Zn (100), whereas a minor reflection at 31.8° was associated with the (200) plane of the silicon substrate.

The observation of several distinct peaks suggests that the deposited ZnO film exhibits polycrystalline characteristics along with a significant level of structural organization. The (101) plane displays the highest intensity among the observed reflections, indicating a favored growth orientation in this direction. Comparable preferential orientation has been observed in thermally oxidized ZnO thin films and is generally linked to the reduction of surface energy throughout the process of crystal growth [16]. The average crystallite size (D) of the ZnO nanostructures was estimated using the Scherrer equation:

$$D = (0.94\lambda)/\beta cos\theta \quad (1)$$

In this context, $\lambda$ represents the X-ray wavelength (1.5406 Å), β denotes the full width at half maximum (FWHM) measured in radians, and $\theta$ indicates the Bragg diffraction angle. The determined crystallite size at an oxidation temperature of 600 °C was around 3.8 nm, affirming the nanocrystalline characteristics of the film. The broadening of the diffraction peaks indicates the presence of small grain size and potential microstrain within the ZnO lattice [18].

The enhancement in peak sharpness and intensity relative to ZnO films produced at lower oxidation temperatures, as documented in related studies, suggests improved crystallinity and a decrease in defect concentration in the thermally treated samples [19]. Such structural features are known to significantly influence the optical and electronic properties of ZnO-based nanomaterials.

A summary of the major diffraction peaks and their corresponding structural parameters is presented in Table 1.

At low magnification (Figure 2(a), ~10,000×), the surface displays a diverse morphology characterized by agglomerated clusters and dispersed nanoparticles (NPs) (≤ 100 nm), which often merge into larger aggregates, resulting in a rough and porous texture. The presence of fine near-spherical NPs alongside larger micron-scale agglomerates suggests a wide range of particle sizes [20].

The presence of rodlike and needlelike crystallites scattered across the surface indicates a tendency for crystal growth along certain crystallographic directions, a phenomenon frequently observed in metal-oxide nanostructures [21]. The presence of inter-particle voids and interconnected channels suggests a significant specific surface area, potentially improving adsorption, catalytic activity, and light–matter interactions [22]. The notable roughness and irregularity of particles align with agglomeration influenced by elevated surface energy in nanostructured materials [23].

Figure 2(b) (high magnification) provides a detailed view of a hierarchical architecture that includes sub-100-nm NPs, clustered domains, and rodlike crystallites. These features are frequently associated with adjustable functional performance in ZnO-based systems [24].

It should be noted that the crystallite size estimated from XRD (~ 3.8 nm) represents coherently diffracting domains, while the larger particle sizes observed in SEM images (< 100 nm) correspond to agglomerated nanostructures composed of multiple crystallites.

Direct SEM characterization of ZnO nanostructures grown on non-PS was not included in the present study, as the focus was placed on elucidating the role of PS on morphology and optical performance. Previous reports indicate that ZnO grown on flat silicon substrates typically exhibits denser and less hierarchical morphologies compared to PS.

The EDX spectrum of the ZnO nanostructures is presented in Figure 3. The identification of Zn and O validates the existence of ZnO [25]. The carbon (C) signal is attributed to the PS substrate and/or carbon coating used for SEM/EDX preparation [26]. The contribution of silicon (Si) is likely derived from the underlying holder or wafer, or from adjacent substrate materials, rather than from the ZnO itself [27]. Table 2 summarizes the corresponding elemental composition obtained by EDX.

The normalized composition reveals that Si, O, and C are the primary elements within the examined volume, aligning with the signal acquisition from the substrate/holder during shallow excitation. In contrast, Zn is present at a low normalized weight percentage, which may be attributed to factors such as thin or porous coverage, surface roughness, or the interaction volume of the beam with the substrate surpassing the ZnO layer [28].

Figure 4 illustrates the optical absorption spectra of ZnO NP thin films. The films demonstrate significant absorption in the UV region while showing minimal absorption in the visible and near-infrared regions, indicating the wide-band-gap characteristics of ZnO [29]. The significant UV absorption is mainly due to

**Table 1**
**Diffraction peaks and their corresponding structural parameters**

| Plane (hkl) | 2θ (°) | FWHM (°) | Crystallite size (nm) | Remarks |
|---|---|---|---|---|
| (002) | 34.6 | 2.20 | 3.8 | ZnO wurtzite |
| (101) | 36.4 | 2.19 | 3.8 | Preferred orientation |
| (102) | 47.6 | 2.25 | 3.7 | Secondary plane |
| (110) | 56.8 | 2.24 | 3.6 | – |

**Figure 2**
**(a) Low-magnification and (b) high-magnification SEM images of ZnO nanostructures grown on PS**

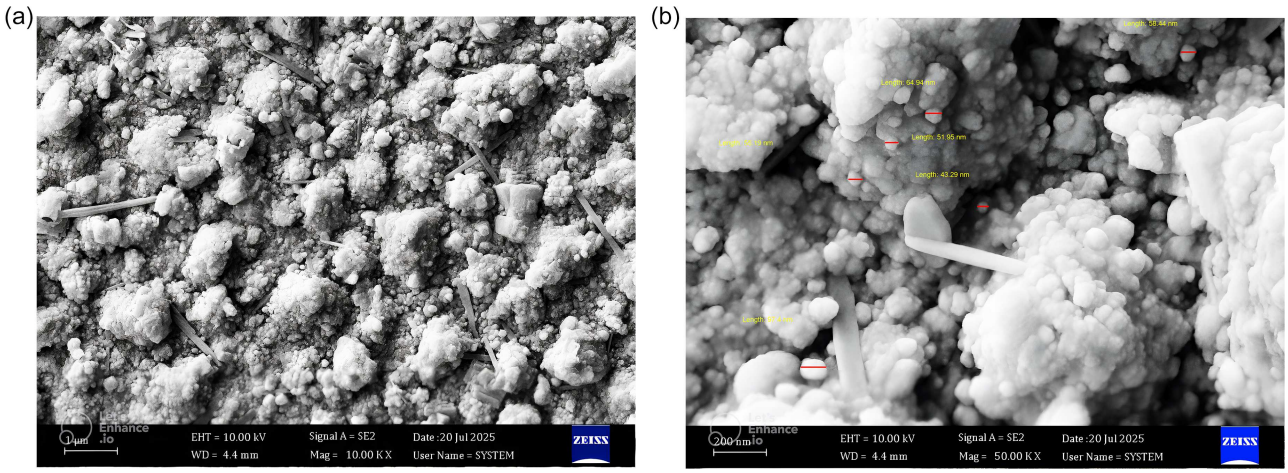


**Figure 3**
**EDX spectrum of ZnO on PS**

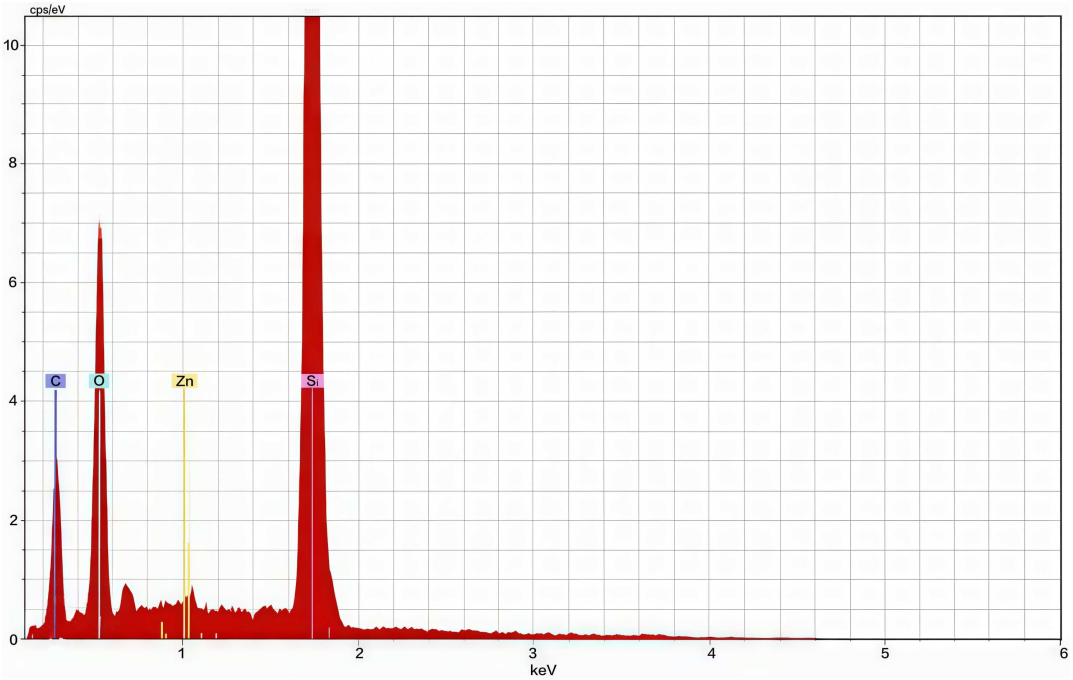


**Table 2**
**EDX elemental composition of the sample**

| Element | Series | unn.C [wt.%] | nom [wt.%] | Atom.[at.%] | Error |
|---|---|---|---|---|---|
| Si 14 | K-series | 124.52 | 83.35 | 72.71 | 6.12 |
| O 8 | K-series | 18.29 | 12.24 | 18.75 | 3.64 |
| C 6 | K-series | 6.19 | 4.14 | 8.45 | 1.83 |
| Zn 30 | L-series | 0.39 | 0.26 | 0.10 | 0.10 |
| Total | – | 149.39 | 100.00 | 100.00 | – |

**Figure 4**
**UV–Vis absorption spectrum of ZnO nanostructured thin film**

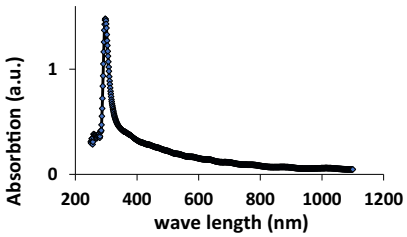


the quantum confinement effect, resulting in a blue shift in the absorption edge as the size of the NP diminishes [30].

The observed blue shift toward higher photon energies suggests an increase in the optical band gap ($E_g$) as grain size decreases, aligning with previous findings by Qutub et al. [31] on ZnO nanostructures. The absorption coefficient ($\alpha$) was used to estimate the optical band gap energy according to Tauc's relation.

The determined band gap energy of the ZnO thin film was around 3.6 eV, as shown in Figure 5, which is marginally greater than the bulk ZnO value (≈ 3.37 eV) attributed to quantum confinement and nanoscale effects [32]. This finding aligns with earlier documented values by Zagorac et al. [33] for ZnO nanostructured thin films, confirming the accuracy of the current measurement.

The broad band gap and significant UV absorption characteristics of ZnO NP thin films position them as highly suitable options for optoelectronic and photovoltaic uses, especially as window or buffer layers in solar cells, where effective UV photon absorption and visibility range transparency are crucial. The significant optical absorption observed in the UV region indicates promising applications in UV photodetectors and photocatalytic systems [34]. The optical properties of the ZnO nanostructured thin films are directly linked to their structural and morphological features as revealed by XRD and SEM analyses. The XRD patterns validated the creation of crystalline ZnO exhibiting a wurtzite structure, whereas the SEM images illustrated NPs under 100 nm in size along with the presence of both rodlike and agglomerated morphologies [23]. The nanoscale dimensions induce quantum confinement effects, which cause a blue shift in the absorption edge and an increase in the optical band gap energy. This elucidates the experimentally determined band gap of approximately 3.6 eV, which is marginally greater than the bulk ZnO value of around 3.37 eV. The smaller grain size and increased surface-to-volume ratio improve the confinement of charge carriers, limiting electron–hole recombination and enhancing photon absorption efficiency [35].

Furthermore, the surface roughness and porosity seen in SEM images lead to increased light scattering, which in turn enhances the effective optical path length within the film and boosts absorption intensity in the UV region [36]. The morphological influence, along with the inherent wide band gap, positions ZnO nanostructures as optimal candidates for UV-sensitive optoelectronic devices and photovoltaic applications [37]. Thus, the reliable correlation between structural refinement and the widening of the optical band gap indicates that the growth parameters employed in this synthesis method effectively yielded high-quality ZnO nanostructures with favorable optical properties for energy and sensing applications [38].

Alongside the optical band gap analysis, the Urbach energy ($E_u$) offers significant insight into the extent of structural disorder and defect-related localized states in semiconductor materials. The exponential segment of the absorption edge, referred to as the Urbach tail, results from photon transitions that engage localized electronic states within the band gap. Localized states are typically produced by structural flaws, lattice vibrations, and compositional changes within the material [39].

Consequently, by examining the exponential tail of the absorption spectrum, one may evaluate the optical quality and crystalline order of ZnO/PS nanostructures. The subsequent picture depicts the fluctuation of the absorption coefficient in relation to photon energy and emphasizes the distinctive Urbach tail region utilized for ascertaining $E_u$ derived from the pronounced absorption edge [40]. Figure 6 shows the relation between the absorption coefficient ($\alpha$) and photon energy ($h\nu$).

Figure 6 shows the absorption coefficient ($\alpha$) for ZnO/PS nanostructures as a function of photon energy ($h\nu$). The graph shows a significant increase around the absorption edge, from which the optical band gap ($E_g$ = 3.6 eV) was calculated, confirming a direct allowed transition in ZnO [41].

An exponential Urbach tail at low photon energies is due to photon transitions caused by localized states caused by structural defects and lattice disorder [42]. The slope of this region determines the Urbach energy ($E_u$), which indicates structural disorder. A sharp edge and small Urbach tail indicate high crystallinity and low defect density in ZnO/PS films. As shown in Figure 7, the obtained $E_u$ value indicates a relatively narrow band-tail width, confirming that the ZnO/PS nanostructures possess a low degree of structural disorder and high optical quality [43].

NLO phenomena are essential in contemporary photonic technologies, facilitating important processes like frequency conversion, optical switching, and optical limiting. Materials that demonstrate significant third-order nonlinearities, such as nonlinear refractive index ($n_2$) and nonlinear absorption coefficients ($\beta$), are especially appealing for applications in photonics, telecommunications, and laser protection [44].

**Figure 5**
**Tauc plot used to determine the optical band gap energy (~3.6 eV)**

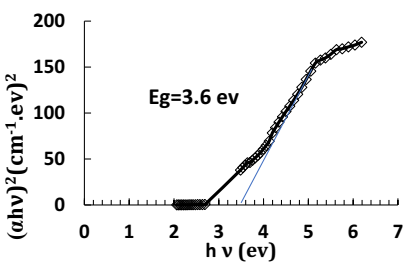


**Figure 6**
**Absorption coefficient ($\alpha$) versus photon energy ($h\nu$)**

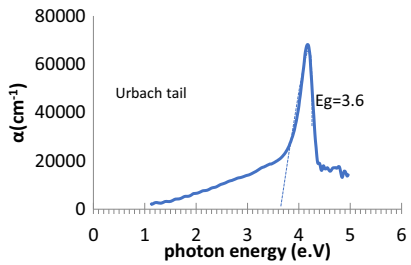

**Figure 7**
**ln($\alpha$) versus photon energy ($h\nu$) plot for estimating Urbach energy ($E_u$) of ZnO/PS nanostructures**

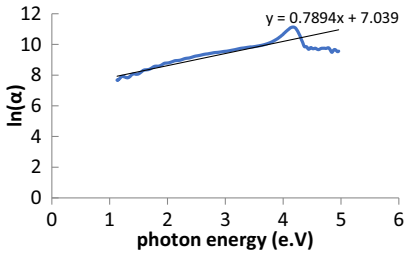


Semiconductor oxides like ZnO have attracted considerable interest as NLO materials because of their broad bandgap, stability in chemical and thermal environments, and capacity to create defect states that can improve nonlinear responses [45].

The NLO properties of the synthesized ZnO nanostructured films were investigated through the Z-scan technique, utilizing both open-aperture (OA) and closed-aperture (CA) configurations, as illustrated in Figure 8.

The transmission curve in the OA mode displayed a clear peak around the focal point ($z \approx +20$ cm), indicative of an SA process. This behavior suggests that the absorption coefficient diminishes as the incident intensity rises, indicating a third-order NLO response that is primarily influenced by nonlinear absorption rather than refraction [46]. The SA effect is commonly associated with defect-related localized energy levels within the band gap, which become saturated at high laser intensities, thereby reducing absorption [47].

In the CA configuration, the curve exhibited minor fluctuations with a nearly constant transmittance (~0.4 mW variation), indicating a weak nonlinear refractive contribution and affirming that the primary NLO mechanism in this film is nonlinear absorption (β) rather than refractive nonlinearity [48].

The improvements in crystallinity, grain refinement, and surface uniformity observed in the ZnO/PS films strongly support their potential integration into wearable electronic and photonic platforms. The high crystallinity and reduced defect density indicated by XRD are essential for achieving stable signal output and low noise levels in wearable strain and pressure sensors. The hierarchical surface morphology revealed by SEM, which includes NPs and rodlike crystallites, provides enhanced surface area and strong light scattering—features that improve UV detection efficiency in skin-mounted photodetectors. The widened optical band gap and strong UV absorption further enable the development of lightweight wearable monitoring devices requiring high spectral

**Figure 8**
**Open- and closed-aperture Z-scan curves of ZnO nanostructured thin film**

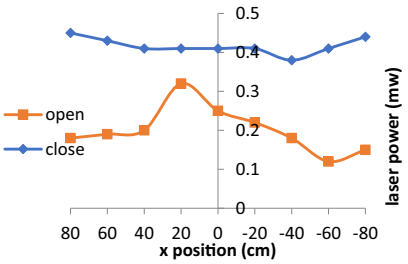


responsivity. Additionally, the prominent SA behavior revealed by Z-scan measurements highlights the suitability of ZnO/PS structures for flexible photonic limiters and NLO modulators that can be embedded into textiles or conformal substrates. Collectively, these results demonstrate that the ZnO/PS nanostructures investigated in this work satisfy key performance requirements for modern wearable technologies.

The observed nonlinear absorption is linked to photo-induced charge carrier transitions occurring between defect states or trap levels, which aligns with the nanocrystalline morphology and porous structure identified in SEM analysis. The defect density and surface states in ZnO nanostructures significantly influence the enhancement of the third-order nonlinear susceptibility ($\chi^3$) and are integral to the optical limiting behavior of the material [46]. Overall, the combination of strong SA, weak nonlinear refraction, and high structural uniformity suggests that the prepared ZnO thin films possess significant potential for photonic, laser safety, and optical limiting applications.

To clarify the role of substrate morphology on NLO behavior, it is worth comparing the present results with reported studies on ZnO nanostructures grown on non-PS substrates. Previous works have shown that ZnO films deposited on flat silicon typically exhibit weaker SA and a more pronounced nonlinear refractive contribution due to reduced surface area and lower density of defect-related localized states. In contrast, the PS substrate used in this study provides abundant nucleation sites and enhanced light–matter interaction, leading to stronger SA behavior and suppressed nonlinear refraction. This comparison highlights the critical role of porous substrates in tailoring the NLO response of ZnO-based nanostructures [48].

It should be noted that the oxidation temperature of 600 °C was selected based on previously reported studies and preliminary optimization trials, indicating its suitability for achieving nanocrystalline ZnO with enhanced structural and optical properties. The present work focuses on providing a detailed correlation between structure, linear optical behavior, and NLO response at a representative oxidation condition rather than claiming a global optimization. A systematic investigation involving different oxidation temperatures and durations will be considered in future studies to further optimize the growth parameters and fully evaluate their influence on the functional performance of ZnO/PS nanostructures.

## 5. Future Work

Future studies will focus on extending the present investigation toward device-oriented and wearable applications. This includes a systematic evaluation of the influence of oxidation temperature and duration on the structural and optical properties of ZnO/PS nanostructures. In addition, mechanical flexibility tests, durability under repeated bending, and biocompatibility assessments will be conducted to validate their suitability for wearable platforms. Further efforts will also explore the integration of ZnO/PS nanostructures onto flexible substrates and their performance in prototype UV photodetectors and nonlinear photonic components. These future efforts are aligned with recent advances in wearable nanostructured materials and flexible optoelectronic systems [49].

## 6. Conclusion

ZnO nanostructured thin films were successfully synthesized on PS substrates using the thermal evaporation–oxidation

technique. XRD analysis confirmed the formation of polycrystalline hexagonal wurtzite ZnO with a preferred (101) orientation and an average crystallite size of approximately 3.8 nm. SEM observations revealed agglomerated NPs and rodlike nanostructures, indicating a rough and porous morphology with high surface area.

Optical characterization showed strong UV absorption with a widened optical band gap (~3.6 eV) attributed to quantum confinement effects, along with a relatively low Urbach energy, indicating good optical quality. Z-scan measurements demonstrated dominant SA with weak nonlinear refraction, highlighting the potential of ZnO/PS nanostructures for photonic and optoelectronic applications. These findings confirm that the employed synthesis approach effectively produces ZnO nanostructures with promising structural, optical, and NLO properties for prospective wearable and photonic devices.

## Ethical Statement

This study does not contain any studies with human or animal subjects performed by any of the authors.

## Conflicts of Interest

The authors declare that they have no conflicts of interest to this work.

## Data Availability Statement

Data are available from the corresponding author upon reasonable request.

## Author Contribution Statement

**Marwa. K. Abood:** Conceptualization, Methodology, Validation, Resources, Project administration. **Wafaa Khalid Khalef:** Conceptualization, Methodology, Validation, Supervision. **Amenah Ali Salman:** Software, Formal analysis. **Nibras Salah Hameed:** Investigation, Data curation, Writing – review & editing. **Mohammed Khalid Khalaf:** Writing – original draft, Visualization.

## References

[1] Ochigbo, S. S., & Sadiku, R. E. (2024). Introduction to the synthesis and characterization of nanostructured materials. In R. Vijayamma, N. Kalarikkal, & S. Thomas (Eds.), *Nanostructured materials for biomedical applications* (pp. 1–34). Elsevier. https://doi.org/10.1016/B978-0-323-90838-2.00004-7

[2] Guo, Y., Liang, Y., Li, Y., Tian, B., Fan, X., He, Y., . . . , & Yao, B. (2024). Optical microcavities empowered biochemical sensing: Status and prospects. *Advanced Devices & Instrumentation*, *5*, 0041. https://doi.org/10.34133/adi.0041

[3] Tsay, C.-Y., Fan, K.-S., Wang, Y.-W., Chang, C.-J., Tseng, Y.-K., & Lin, C.-K. (2010). Transparent semiconductor zinc oxide thin films deposited on glass substrates by sol–gel process. *Ceramics International*, *36*(6), 1791–1795. https://doi.org/10.1016/j.ceramint.2010.03.005

[4] Kim, K. H., Utashiro, K., Abe, Y., & Kawamura, M. (2014). Structural properties of zinc oxide nanorods grown on Al-doped zinc oxide seed layer and their applications in dye-sensitized solar cells. *Materials*, *7*(4), 2522–2533. https://doi.org/10.3390/ma7042522

[5] Toma, F. T. Z., Rahman, M. S., & Maria, K. H. (2025). A review of recent advances in ZnO nanostructured thin films by various deposition techniques. *Discover Materials*, *5*(1), 60. https://doi.org/10.1007/s43939-025-00201-1

[6] Gupta, B., Jain, A., & Mehra, R. M. (2010). Development and characterization of sol-gel derived Al doped ZnO/p-Si photodiode. *Journal of Materials Science & Technology*, *26*(3), 223–227. https://doi.org/10.1016/S1005-0302(10)60037-0

[7] Kaim, P., Lukaszkowicz, K., Szindler, M., Szindler, M. M., Basiaga, M., & Hajduk, B. (2021). The influence of magnetron sputtering process temperature on ZnO thin-film properties. *Coatings*, *11*(12), 1507. https://doi.org/10.3390/coatings11121507

[8] Fasquelle, D., Deputier, S., Bouquet, V., & Guilloux-Viry, M. (2022). Effect of the microstructure of ZnO thin films prepared by PLD on their performance as toxic gas sensors. *Chemosensors*, *10*(7), 285. https://doi.org/10.3390/chemosensors10070285

[9] Suhail, H. S., & Abdulridha, A. R. (2024). Preparation and characterization of thin films bismuth (III) oxide/zinc oxide nanostructures prepared by thermal evaporation technique as gas sensor applications. *Transactions on Electrical and Electronic Materials*, *25*(1), 1–14. https://doi.org/10.1007/s42341-023-00490-4

[10] Abdallah, B., Kakhia, M., & Obaide, A. (2021). Morphological and structural studies of ZnO nanotube films using thermal evaporation technique. *Plasmonics*, *16*(5), 1549–1556. https://doi.org/10.1007/s11468-021-01420-x

[11] Cheng, Z., Lin, H., Liu, Y., Yan, Q., Su, B.-L., & Zhang, H. (2025). A Stress-buffering hierarchically porous silicon/carbon composite for high-energy lithium-ion batteries. *Advanced Functional Materials*. https://doi.org/10.1002/adfm.202505207

[12] Abood, M. K., Fayad, M. A., Al Salihi, H. A., & Salbi, H. A. A. (2021). Effect of ZnO nanoparticles deposition on porous silicon solar cell. *Materials Today: Proceedings*, *42*, 2935–2940. https://doi.org/10.1016/j.matpr.2020.12.771

[13] Mutar, Z. S., & Mutlak, F. A.-H. (2025). Fabrication and characterization of zinc oxide nanoparticles deposited on porous silicon as a photodetector and solar cell. *Journal of Optics*. https://doi.org/10.1007/s12596-025-02597-8

[14] Zhou, J., Chen, H., Fu, K., & Zhao, Y. (2021). Gallium oxide-based optical nonlinear effects and photonics devices. *Journal of Materials Research*, *36*(23), 4832–4845. https://doi.org/10.1557/s43578-021-00397-x

[15] Wang, L.-Y., Shi, B.-Y., Yao, C.-B., Wang, Z.-M., Wang, X., Jiang, C.-H., . . . , & Song, Y.-L. (2023). Size and morphology modulation in ZnO nanostructures for nonlinear optical applications: a review. *ACS Applied Nano Materials*, *6*(12), 9975–10014. https://doi.org/10.1021/acsanm.3c01509

[16] Abdulrahman, A. F., Ahmed, S. M., Hamad, S. M., & Barzinjy, A. A. (2021). Effect of growth temperature on morphological, structural, and optical properties of ZnO nanorods using modified chemical bath deposition method. *Journal of Electronic Materials*, *50*(3), 1482–1495. https://doi.org/10.1007/s11664-020-08705-7

[17] Salim, E. T., Saimon, J. A., Abood, M. K., & Alsultany, F. H. (2024). A preliminary study on structural and optical properties of heat treated Nb2O5 nanostructure. *International Journal of Nanoelectronics and Materials*, *16*(1), 21–32. https://doi.org/10.58915/ijneam.v16i1.910

[18] Etcheverry, L. P., Flores, W. H., L da Silva, Douglas, & Moreira, E. C. (2018). Annealing effects on the

structural and optical properties of ZnO nanostructures. *Materials Research*, *21*(2), e20170936. https://doi.org/10.1590/1980-5373-MR-2017-0936

[19] Sener, E., Bayram, O., Hasar, U. C., & Simsek, O. (2021). Structural and optical properties of RF sputtered ZnO thin films: Annealing effect. *Physica B: Condensed Matter*, *605*, 412421. https://doi.org/10.1016/j.physb.2020.412421

[20] Hajos, M., Starowicz, M., Brzychczyk, B., Basista, G., & Francik, S. (2025). Size distribution of zinc oxide nanoparticles depending on the temperature of electrochemical synthesis. *Materials*, *18*(2), 458. https://doi.org/10.3390/ma18020458

[21] Morales-Morales, F., Martínez-Ayala, L., Jiménez-Vivanco, M. R., & Gómez-Pozos, H. (2023). Zno deposition on silicon and porous silicon substrate via radio frequency magnetron sputtering. *Coatings*, *13*(11), 1839. https://doi.org/10.3390/coatings13111839

[22] Puri, S., Kalkan, A. K., & McIlroy, D. N. (2025). Hierarchical Design of high-surface-area zinc oxide nanorods grown on one-dimensional nanostructures. *Sci*, *7*(3), 114. https://doi.org/10.3390/sci7030114

[23] Raha, S., & Ahmaruzzaman, M. (2022). ZnO nanostructured materials and their potential applications: Progress, challenges and perspectives. *Nanoscale Advances*, *4*(8), 1868–1925. https://doi.org/10.1039/D1NA00880C

[24] Duan, Y., Li, C., Ye, Z., Li, H., Yang, Y., Sui, D., & Lu, Y. (2022). Advances of carbon materials for dual-carbon lithium-ion capacitors: A review. *Nanomaterials*, *12*(22), 3954. https://doi.org/10.3390/nano12223954

[25] Rusli, N. I., Abdulgafour, H., Hassan, Z., Yam, F. K., Ali, N. K., Hashim, A. M., . . . , & Nayan, N. (2012). ZnO nanostructures grown on porous silicon substrate without catalyst. In *2012 International Conference on Enabling Science and Nanotechnology*, 1–2. https://doi.org/10.1109/ESciNano.2012.6149704

[26] Hector, D., Olivero, S., Orange, F., Duñach, E., & Gal, J.-F. (2019). Quality control of a functionalized polymer catalyst by energy dispersive X-ray spectrometry (EDX or EDS). *Analytical Chemistry*, *91*(3), 1773–1778. https://doi.org/10.1021/acs.analchem.8b04170

[27] Abdallah, B., Hussin, R., & Zetoune, W. (2022). Effect of etched silicon substrate on structural, morphological, and optical properties of deposited ZnO films via DC sputtering. *Aerosol Science and Engineering*, *6*(1), 30–44. https://doi.org/10.1007/s41810-021-00122-5

[28] Savaloni, H., & Savari, R. (2018). Nano-structural variations of ZnO: N thin films as a function of deposition angle and annealing conditions: XRD, AFM, FESEM and EDS analyses. *Materials Chemistry and Physics*, *214*, 402–420. https://doi.org/10.1016/j.matchemphys.2018.04.099

[29] Singh, S., Gade, J. V., Verma, D. K., Elyor, B., & Jain, B. (2024). Exploring ZnO nanoparticles: UV–visible analysis and different size estimation methods. *Optical Materials*, *152*, 115422. https://doi.org/10.1016/j.optmat.2024.115422

[30] Xu, J.-J., Lu, Y.-N., Tao, F.-F., Liang, P.-F., & Zhang, P.-A. (2023). ZnO nanoparticles modified by carbon quantum dots for the photocatalytic removal of synthetic pigment pollutants. *ACS Omega*, *8*(8), 7845–7857. https://doi.org/10.1021/acsomega.2c07591

[31] Qutub, N., Singh, P., Sabir, S., Sagadevan, S., & Oh, W.-C. (2022). Enhanced photocatalytic degradation of Acid Blue dye using CdS/TiO2 nanocomposite. *Scientific Reports*, *12*(1), 5759. https://doi.org/10.1038/s41598-022-09479-0

[32] Chiang, W., Morshed, O., & Krauss, T. (2023). *Quantum confined semiconductor nanocrystals*. USA: American Chemical Society. https://doi.org/10.1021/acsinfocus.7e7022

[33] Zagorac, D., Zagorac, J., Pejić, M., Matović, B., & Schön, J. C. (2022). Band gap engineering of newly discovered ZnO/ZnS polytypic nanomaterials. *Nanomaterials*, *12*(9), 1595. https://doi.org/10.3390/nano12091595

[34] Gartner, M., Stroescu, H., Mitrea, D., & Nicolescu, M. (2023). Various applications of ZnO thin films obtained by chemical routes in the last decade. *Molecules*, *28*(12), 4674. https://doi.org/10.3390/molecules28124674

[35] Aellen, M., & Norris, D. J. (2022). Understanding optical gain: Which confinement factor is correct? *ACS Photonics*, *9*(11), 3498–3505. https://doi.org/10.1021/acsphotonics.2c01222

[36] Kumar, P., Nisha, Sarkar, P., Singh, S., Mishra, K., B. C., & Katiyar, R. S. (2022). The influence of post-growth heat treatment on the optical properties of pulsed laser deposited ZnO thin films. *Applied Physics A*, *128*(5), 372. https://doi.org/10.1007/s00339-022-05511-2

[37] Shahzad, S., Javed, S., & Usman, M. (2021). A review on synthesis and optoelectronic applications of nanostructured ZnO. *Frontiers in Materials*, *8*, 613825. https://doi.org/10.3389/fmats.2021.613825

[38] Singh, J., & Srivastava, A. (2022). Morphological evolution and its correlation with optical and field emission properties in pulsed laser deposited ZnO nanostructures. *Materials Science in Semiconductor Processing*, *138*, 106282. https://doi.org/10.1016/j.mssp.2021.106282

[39] Ghobadi, N., Sohrabi, P., & Hatami, H. R. (2020). Correlation between the photocatalytic activity of CdSe nanostructured thin films with optical band gap and Urbach energy. *Chemical Physics*, *538*, 110911. https://doi.org/10.1016/j.chemphys.2020.110911

[40] Riungu, G. G., Mugo, S. W., Ngaruiya, J. M., John, G. M., & Mugambi, N. (2021). Optical band energy, Urbach energy and associated band tails of nano crystalline TiO2 films at different annealing rates. *American Journal of Nanosciences*, *7*(1), 28–34. https://doi.org/10.11648/j.ajn.20210701.15

[41] Özgür, Ü., Alivov, Y. I., Liu, C., Teke, A., Reshchikov, M. A., Doğan, S., . . . , & Morkoç, H. (2005). A comprehensive review of ZnO materials and devices. *Journal of Applied Physics*, *98*(4), 041301. https://doi.org/10.1063/1.1992666

[42] Ligatchev, V. (2024). On nature of Urbach's tail in optical absorption spectrum of nano-crystalline zinc oxide (nc-ZnO). *AIP Conference Proceedings*, *2924*(1), 050002. https://doi.org/10.1063/5.0182013

[43] Benny, D. P., Munya, V., Ghosh, A., Kumar, R., Pal, D., Pfnür, H., & Chattopadhyay, S. (2023). Self-healing of defect-mediated disorder in ZnO thin films grown by atomic layer deposition. *Journal of Electronic Materials*, *52*(12), 8293–8302. https://doi.org/10.1007/s11664-023-10758-3

[44] Mathai, J., Jose, A. K., Anjana, M. P., Aleena, P. A., Kunjumon, J., Ittyachan, R., . . . , & Sajan, D. (2023). Substantial effect of Cr doping on the third-order nonlinear optical properties of ZnO nanostructures. *Optical Materials*, *142*, 114128. https://doi.org/10.1016/j.optmat.2023.114128

[45] Lü, Y., Chen, Z., Shi, F., Li, Z., Xiao, Z., Wu, X., . . . , & Fang, Y. (2025). Enhanced broadband non-degenerate two-photon absorption in Ga-doped ZnO for ultrafast all-optical

switching. *Chinese Optics Letters*, *23*(11), 111901. https://doi.org/10.3788/COL202523.111901

[46] Wang, L.-Y., Shi, B.-Y., Yao, C.-B., Wang, Z.-M., Wang, X., Jiang, C.-H., . . . , & Song, Y.-L. (2023). Size and morphology modulation in ZnO nanostructures for nonlinear optical applications: A review. *ACS Applied Nano Materials*, *6*(12), 9975–10014. https://doi.org/10.1021/acsanm.3c01509

[47] Menon, P. S., Anjana, M. P., Jose, A. K., Kunjumon, J., A, P., A, Chandran., S, Sajan, D., . . . , Sajan, D. (2022). The role of defects on linear and nonlinear optical properties of pristine and nickel doped zinc oxide nanoparticles. *Surfaces and Interfaces*, *34*, 102393. https://doi.org/10.1016/j.surfin.2022.102393

[48] Abdallah, B., Zidan, M. D., & Allahham, A. (2021). Syntheses, structural and nonlinear optical characteristics of ZnO films using Z-scan technique. *Silicon*, *13*(11), 4139–4146. https://doi.org/10.1007/s12633-020-00702-z

[49] Huang, J., Xu, B., Gao, Y., Jiang, C., Guan, X., Li, Z., . . . , & (2022). Surface microstructural engineering of continuous fibers as one-dimensional multifunctional fiber materials for wearable electronic applications. *Chemical Engineering Journal*, *446*, 137192. https://doi.org/10.1016/j.cej.2022.137192

**How to Cite:** Abood, M. K., Khalef, W. K., Salman, A. A., Hameed, N. S., & Khalaf, M. K. (2026). Structural, Optical, and Nonlinear Optical Properties of ZnO Nanostructures Grown on Porous Silicon. *Smart Wearable Technology*. https://doi.org/10.47852/bonviewSWT62028665